Accurate Retrieval of Structural Information from Laser-Induced Photoelectron and High-Order Harmonic Spectra by Few-Cycle Laser Pulses

Toru Morishita,[1,2] Anh-Thu Le,[1] Zhangjin Chen,[1] and C. D. Lin[1]

[1]*Department of Physics, Cardwell Hall, Kansas State University, Manhattan, Kansas 66506, USA*
[2]*Department of Applied Physics and Chemistry, University of Electro-Communications,*
1-5-1 Chofu-ga-oka, Chofu-shi, Tokyo, 182-8585, Japan
and PRESTO, Japan Science and Technology Agency, Kawaguchi, Saitama 332-0012, Japan
(Received 19 July 2007; published 8 January 2008)

By analyzing accurate theoretical results from solving the time-dependent Schrödinger equation of atoms in few-cycle laser pulses, we established the general conclusion that laser-generated high-energy electron momentum spectra and high-order harmonic spectra can be used to extract accurate differential elastic scattering and photo-recombination cross sections of the target ion with *free* electrons, respectively. Since both electron scattering and photoionization (the inverse of photo-recombination) are the conventional means for interrogating the structure of atoms and molecules, this result implies that existing few-cycle infrared lasers can be implemented for ultrafast imaging of transient molecules with temporal resolution of a few femtoseconds.

Electron diffraction and x-ray diffraction are the conventional methods for imaging molecules to achieve spatial resolution of better than sub-Angstroms, but they are incapable of achieving temporal resolutions of femto- to tens of femtoseconds, in order to follow chemical and biological transformations. To image such transient events, unique facilities like ultrafast electron diffraction method [1] or large facilities such as x-ray free-electron lasers (XFELs) are being developed. Instead of pursuing these evolving technologies, here we provide the needed quantitative analysis to show that existing few-cycle infrared lasers may be implemented for ultrafast imaging of transient molecules.

When an atom is exposed to an infrared laser, the atom is first tunnel ionized with the release of an electron. This electron is placed in the oscillating electric field of the laser and may be driven back to revisit its parent ion. This reencounter incurs various elastic and inelastic electron-ion collision phenomena where the structural information of the target is embedded [2,3]. The possibility of using such laser-induced returning electrons for self-imaging molecules has been discussed frequently in the past. Theoretical studies of laser-induced electron momentum images of simple molecules do show interference maxima and minima typical of diffraction images, but they are observed only for large internuclear distances [4–8]. Furthermore, the role of laser fields on these diffraction images has been shown to be quite complicated [5]. Recently, it was reported that the outermost molecular orbital of the N_2 molecule can be extracted from the high-order harmonic generation (HHG) spectra using the tomographic procedure [9]. This interesting result has generated a lot of excitement, but the reported results are obtained based on a number of assumptions [10–12]. To make dynamic chemical imaging with infrared lasers as a practical tool, general theoretical considerations, especially the validity of the extraction procedure, should be examined carefully.

In this Letter, we show that elastic scattering cross sections of the target ion by free electrons can be accurately extracted from laser-induced photoelectron momentum spectra. We also show that accurate photo-recombination cross sections of the target ion can be extracted from the HHG spectra. Our conclusions are based on accurate theoretical results by solving the time-dependent Schrödinger equations (TDSE) of atoms in intense laser fields. While these conclusions are derived from atomic targets, the same conclusions are expected to apply to molecular targets as well (where accurate TDSE calculations are very difficult). For molecules, these results have far-reaching implications. Both elastic scattering and photoionization are the standard tools for studying the structure of atoms and molecules in conventional energy domain measurements; thus, high-energy photoelectrons and high harmonics generated by infrared lasers offer the promise for revealing the structure of the target, with the added advantage of temporal resolution down to a few femtoseconds offered by few-cycle pulses.

Consider a typical few-cycle laser pulse, with mean wavelength of 800 nm and peak intensity of 10^{14} W/cm^2. The electric field $\boldsymbol{F}(t) = -\partial \boldsymbol{A}(t)/\partial t$ and the vector potential $\boldsymbol{A}(t)$ of such a laser pulse are depicted in Fig. 1(a). By placing a hydrogen atom in such a laser pulse, we solved the TDSE to obtain the photoelectron energy and momentum distributions, shown in Figs. 1(b) and 1(c), respectively. Figure 1(d) shows the electron momentum image of Ar in the same laser pulse. The theoretical method for solving the TDSE has been described previously [13,14].

In Fig. 1(b), two particular energies, $2U_p$ and $10U_p$, are marked, where $U_p = A_0^2/4$ is the ponderomotive energy, with A_0 being the peak value of the vector potential of the
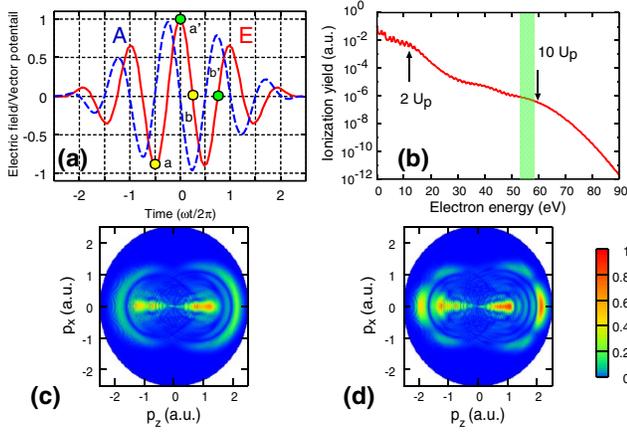
FIG. 1 (color online). (a) Schematic of the electric field (E) and the vector potential (A) of a typical few-cycle pulse. (b) Electron energy spectra of atomic hydrogen ionized by a 5 fs (FWHM) laser pulse, with mean wavelength of 800 nm and peak intensity at 10^{14} W/cm^2. (c) Normalized 2D photoelectron momentum spectra of atomic hydrogen. The images are renormalized for each photoelectron energy to reveal the global angular distributions. (d) Momentum images of Ar in the same pulse.

laser pulse. (We use atomic units in this Letter.) According to the classical estimate, the electron can reach up to $2U_p$ if it is released by the laser field alone. It can reach up to $10U_p$ if the returning electron is back scattered by the parent ion [15,16]. To display the full electron momentum image surface in a single plot, in Figs. 1(c) and 1(d), we normalized electron momentum distributions such that the total ionization yield at each electron energy is the same. We have chosen the horizontal axis to be along the direction of the laser's polarization and the vertical axis along any direction perpendicular to it (due to cylindrical symmetry of the linearly polarized light).

For this Letter, we only focus on the two outermost half circular rings, one on the "left" and another on the "right," of Fig. 1(c). Note that the center of each circle is shifted from the origin. We will call these circular rings back rescattered ridges (BRR), representing electrons that have been rescattered into the backward directions by the target ion. The BRR on the "right" is from electrons born at time near "a" [Fig. 1(a)], travelling to the right and then returning to the target ion at time near "b," where they are rescattered back to the right. Each momentum half circle is represented approximately by $A_r\hat{p}_z + p_0\hat{p}_r$, where the second term is the momentum of the backscattered electron and the first term is the momentum added to the electron as it propagates from "b" to the end of the laser pulse. The magnitude of the momentum p_0 is related to the ponderomotive energy by $3.17\bar{U}_p = p_0^2/2$ (where $\bar{U}_p = A_r^2/4$, and A_r is the vector potential at "b"), which is the maximum energy of electrons that return to revisit the parent ion. For back scattered electrons, the two momen-

tum terms add to give high-energy photoelectrons, reaching a maximum of $10U_p$ for electrons that have been scattered by 180° [16]. If the electrons are scattered into the forward direction, the two momentum terms subtract from each other, resulting in lower energy electrons. Similar BRR electrons are found on the left. These are from electrons that were born near "a'" and were rescattered back to the left near "b'" [Fig. 1(a)]. Both the shift of the center and the radius are smaller due to rescattering occurring near "b'" where the vector potential is smaller.

In Figs. 1(c) and 1(d), we note that the positions of the BRR are very close to each other, but the yields on the BRR for H and Ar are quite different, where the former is monotonic while the latter has a clear minimum. Taking the actually calculated photoelectron yields (without the normalization as shown in the figure), we compare the angular dependence of the intensities along BRR with the elastic differential cross sections of the target ion by *free* electrons at energy $E = p_0^2/2$. The results are shown in Fig. 2(a) for H target and 2(b) for Ar, where the scattering angles are measured from the direction of the "incident" electron beam. Good agreement between the two results for each target atom can be seen. Such good agreement has been duplicated at different laser intensities and other atomic systems [see Ne and Xe in Figs. 2(c) and 2(d), respectively.]. Note that differential cross sections at smaller scattering angles are not used in the analysis since they are "contaminated" by rescattering into the forward directions from the other side (i.e., rescattering at "b'" [Fig. 1(a)]). These comparisons illustrate that laser-induced momentum images on the BRR can be used to obtain elastic scattering cross sections of free electrons by the target ion. For atomic hydrogen, the elastic scattering cross section is given by the Rutherford formula. For other atomic ions, partial wave phase shifts are calculated to
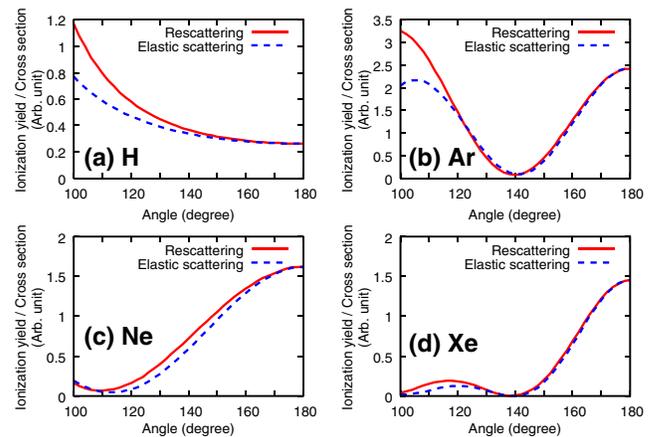

FIG. 2 (color online). Angular distributions of photoelectrons along the BRR compared to the differential elastic scattering cross sections of the target ion. Each BRR is taken to be the outer half circle on the right side of Figs. 1(c) and 1(d), respectively. (a) for H target, (b) for Ar, (c) for Ne, (d) for Xe.

obtain the differential cross sections. The minima are due to diffraction of electrons by the core potential and have been observed in electron-ion collision experiments [17]. We comment that these high-energy photoelectron momentum spectra have been experimentally observed earlier [15], but there has been no quantitative analysis.

According to the intuitive rescattering model, photoelectron yields along the BRR may be attributed to back scattering of the returning electron wave packet. To test this idea, we write the photoelectron momentum yields $I(\boldsymbol{p})$ along the BRR by $I(\boldsymbol{p}) = \sigma(p_0, \theta)F(p_0, \theta)$, with $\boldsymbol{p} = A_r\hat{\boldsymbol{p}}_z + p_0\hat{\boldsymbol{p}}_r$, where $\sigma(p_0, \theta)$ is the elastic differential cross section for each ion by a free electron with energy $E = p_0^2/2$, and θ is the scattering angle of the free electron.

In Fig. 3(a), we show the extracted $F(p_0, \theta)$ from H at two different angles. They are essentially identical such that we may identify $F(p_0) = F(p_0, \theta)$ as the wave packet of the returning electrons with momentum near p_0. Note that the wave packet extracted from Ar target, as shown in Fig. 3(b), is essentially identical to Fig. 3(a) except for a small shift of the center from $p_0 = 1.22$ to 1.25. The width of the wave packet is found to be independent of the target. In Fig. 3(c), we show that $F(p_0) = F(p_0, \theta)$ indeed holds well for electrons that have been back scattered for angles larger than about 130°. Note that a separate electron wave packet can be retrieved from the photoelectron momentum spectra measured on the "left." The wave packet analyzed above is for a 5 fs (FWHM) pulse with the carrier-envelope phase (CEP) $\phi = 0$. The returning electron wave packet depends on the CEP. For long pulses, electron yields on each BRR will exhibit oscillations characteristic of ATI peaks, but elastic scattering cross sections by free electrons can still be extracted from the smooth envelope of the momentum images [18].
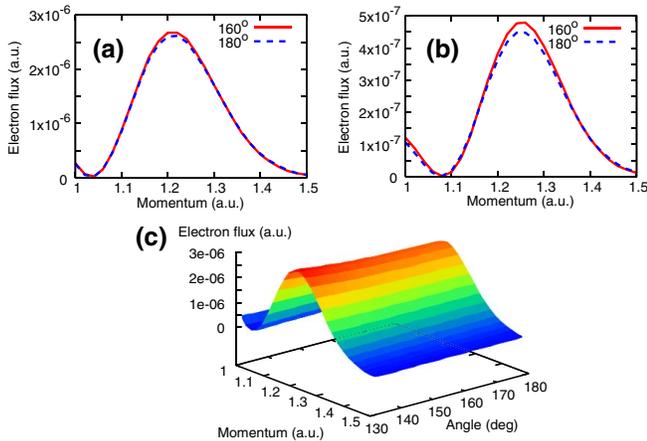

FIG. 3 (color online). Electron wave packets extracted from photoelectron momentum images along the BRR are shown to be identical for scattering angles of 160° and 180°, extracted from (a) H target, (b) Ar target, using the same ionizing laser. (c) The extracted electron wave packet from H target is the same over the angular range of 130° to 180°.

The above results, based on the exact solution of TDSE, clearly established that electron yields on the BRR can be viewed as the backscattering of the returning electron wave packet. According to the three-step model, HHG is due to photo-recombination of the same returning electrons. Since the returning electron wave packets have been shown to be largely independent of target atoms (except for a normalization) for the same laser pulse, the difference in the HHG spectra can be attributed to the recombination cross sections. To check this idea, we compare HHG from Ne with a companion atom that has the same ionization potential such that the cutoff energies will be identical. The latter was chosen to be a model hydrogen atom with the effective charge chosen such that its $1s$ binding energy is the same as the $2p$ binding energy of Ne. By solving the TDSE, we obtain the HHG spectra, respectively, for the two atoms in a 5.2 fs laser pulse, with mean wavelength of 1064 nm and peak intensity of 2×10^{14} W/cm². The longer wavelength was used in order to span a larger photon energy range in the generated harmonics. From the calculated HHG yield, we divide each by the calculated photo-recombination cross section (PRCS) of each atom. In Fig. 4(a), we compare the resulting "electron wave packets" (normalized) vs the HHG order. Clearly, the two electron wave packets are very close to each other, showing that differences in the HHG spectra between the
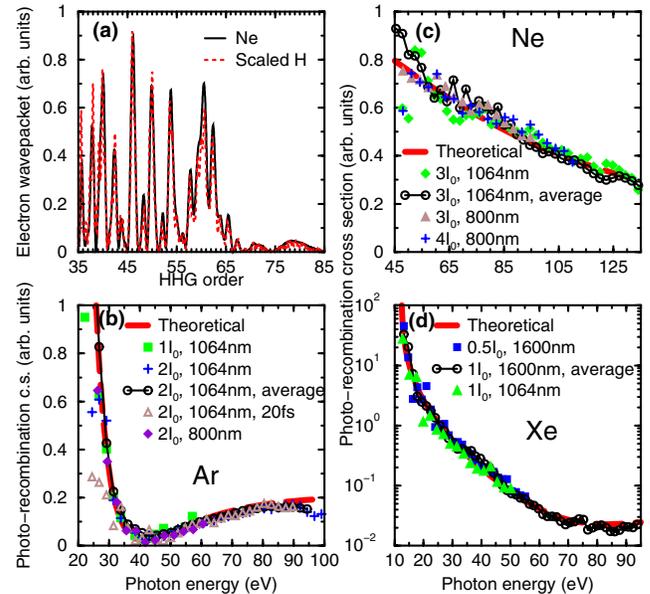

FIG. 4 (color online). (a) Comparison of the "electron wave packets" extracted from the HHG spectra of Ne and scaled H generated by a 5.2 fs laser pulse with peak intensity of 2×10^{14} W/cm² and mean wavelength of 1064 nm. Extracted photo-recombination cross sections from the HHG, of Ar (b), Ne (c) and Xe (d), using different laser pulses, plotted vs the photon energy. For each panel, the dashed red line denotes the calculated photo-recombination cross sections by free electrons. ($I_0 = 10^{14}$ W/cm².)

two targets are due to the different PRCS. We comment that dipole matrix elements in the PRCS are calculated using accurate continuum states with outgoing wave boundary conditions. Both the ground and continuum wave functions are solved from the same model potential, and the kinetic energy of the electron is related to the photon energy by $\hbar\omega = k^2/2 + I_p$. For one-electron atoms, such cross sections can be easily calculated [19].

The good agreement in the deduced "electron wave packet" in Fig. 4(a) prompts us to ask whether one can obtain accurate PRCS from the HHG spectra of an unknown target by comparing it with the HHG spectra from a known atom with identical or nearly identical ionization potential. For this purpose, we generated HHG spectra for Ar and scaled H atoms, with the charge of H chosen to have identical ionization potential as Ar. Different laser intensities and wavelengths were used to generate HHG from which the PRCS of Ar are derived. If the procedure is valid, the extracted PRCS should be independent of the lasers used, except for the range of photon energies covered. In Fig. 4(b), we compare the extracted cross sections from the HHG generated by various laser pulses with the accurate PRCS directly calculated for Ar. One can see that the deduced values scatter nicely around the calculated one. The fluctuation of the extracted cross sections can be reduced if the HHG intensity is taken from the averaged HHG *amplitudes* with nearby laser intensities. Thus, the smooth black line is obtained from averaging over 11 intensities within $\pm 5\%$ of the mean intensity of 2×10^{14} W/cm^2. This coherent averaging sharpens the odd harmonics and reduces the harmonic yields in between, similar to the effect of propagation of HHG in the medium. Note that in calculating PRCS, we include dipole transitions from $3p$ to both s and d continuum states. The minimum in the cross section occurs near the Cooper minimum where the d-wave electric dipole moment changes sign. From Fig. 4(b), we can say that accurate PRCS indeed can be extracted from the HHG yields. Similar test showing good agreement has been made also on Ne and Xe atoms [Figs. 4(c) and 4(d)], again using scaled hydrogen as the companion atoms.

In this Letter, we have identified the spectral region where the *nonlinear* laser-atom interaction can be simplified to extract the *linear* interaction between a returning electron wave packet with the atomic ion. Even though the results were presented only for atomic targets, we expect the same simplifications hold for molecular targets. For

molecules, this opens up the exciting possibility of using infrared lasers for ultrafast imaging of molecules that are undergoing structural transformation. Both elastic electron scattering and photoionization (the inverse of photo-recombination) are the well-tested means for probing the structure of molecules, and from such data, structural information can be deduced. In conclusion, we have established the theoretical foundation for carrying out structural analysis of molecules with infrared lasers. If this road map is implemented experimentally, table-top infrared lasers would offer a very competitive new technology for ultrafast time-resolved chemical imaging, with temporal resolution down to a few femtoseconds.

[1] A. Zewail, Annu. Rev. Phys. Chem. **57**, 65 (2006).
[2] K. Schafer *et al.*, Phys. Rev. Lett. **70**, 1599 (1993).
[3] P. Corkum, Phys. Rev. Lett. **71**, 1994 (1993).
[4] T. Zuo *et al.*, Chem. Phys. Lett. **259**, 313 (1996).
[5] M. Spanner *et al.*, J. Phys. B **37**, L243 (2004).
[6] S. X. Hu and L. A. Collins, Phys. Rev. Lett. **94**, 073004 (2005).
[7] M. Lein *et al.*, Phys. Rev. A **66**, 051404(R) (2002).
[8] S. N. Yurchenko *et al.*, Phys. Rev. Lett. **93**, 223003 (2004).
[9] J. Itatani *et al.*, Nature (London) **432**, 867 (2004).
[10] V. H. Le *et al.*, Phys. Rev. A **76**, 013414 (2007).
[11] S. Patchkovskii *et al.*, Phys. Rev. Lett. **97**, 123003 (2006).
[12] J. Levesque *et al.*, Phys. Rev. Lett. **98**, 183903 (2007).
[13] Z. Chen *et al.*, Phys. Rev. A **74**, 053405 (2006).
[14] T. Morishita *et al.*, Phys. Rev. A **75**, 023407 (2007).
[15] B. Yang *et al.*, Phys. Rev. Lett. **71**, 3770 (1993).
[16] G. G. Paulus *et al.*, J. Phys. B **27**, L703 (1994).
[17] J. B. Greenwood, I. D. Williams, and P. McGuinness, Phys. Rev. Lett. **75**, 1062 (1995).
[18] Z. Chen *et al.*, Phys. Rev. A **76**, 043402 (2007).
[19] U. Fano and J. W. Cooper, Rev. Mod. Phys. **40**, 441 (1968). See Section 4.